Computer Assisted Mechanics and Engineering Sciences, 9: 489–517, 2002.

Numerical simulation of an explosion in a simple scale model of a nuclear reactor[1]

Marie-France Robbe and Michel Lepareux
CEA Saclay, SEMT-DYN, 91191 Gif sur Yvette cedex, France

Eloi Treille
Socotec Industrie, 1 av. du Parc, 78180 Montigny le Bretonneux, France

Yves Cariou
Novatome, NVPM,10 rue Juliette Récamier, 69006 Lyon, France

(Received Februay 9, 2001)

In the case of a Hypothetical Core Disruptive Accident (HCDA) in a Liquid Metal Fast Breeder Reactor, it is assumed that the core of the nuclear reactor has melted partially and that the chemical interaction between molten fuel and liquid sodium creates a high pressure gas bubble in the core. The violent expansion of this bubble loads and deforms the reactor vessel, thus endangering the safety of the nuclear plant. The experimental test MARA 8 simulates the explosive phenomenon in a mock-up enclosed in a flexible vessel with a flexible roof. This paper presents a numerical simulation of the test and a comparison of the computed results with the experimental results and previous numerical ones.

1. INTRODUCTION

To ensure a high safety level in French nuclear power plants, safety authorities require plant designers to take into consideration several cases of hypothetical severe accidents which the plant must be able to withstand. The aim is to guarantee that even a core-melt accident would not require any stringent countermeasures such as evacuation or relocation of the population beyond the immediate vicinity of the plant.

For the Liquid Metal Fast Breeder Reactors (LMFBR), one of the severe accidents envisaged is a Hypothetical Core Disruptive Accident (HCDA). The scenario supposes that an accident has occurred in which the reactor core has partially melted. The chemical interaction of molten fuel with the liquid sodium used to cool the reactor core very quickly produces a high quantity of gaseous components.

A high pressure gas bubble forms in the core centre. The explosive expansion of this bubble leads to overloading of the reactor vessel and its internal structures. To avoid the release of radioactive products into the plant containment, the integrity of the reactor vessel must be maintained.

During the 70s and 80s, several countries contributed to the understanding of the consequences of a HCDA. They undertook several experimental programmes or developed computer codes especially devoted to the analysis of the transient loads resulting from a HCDA. The computer codes generally aimed at simulating a HCDA in the reactor in order to demonstrate its capacity to withstand such an accident. The experimental programmes had more varied objectives.

[1]This is an extended version of the article presented at the 8th International Conference on Numerical Methods in Continuum Mechanics, Liptovský Ján, Low Tatras, Slovakia, September 19–24, 2000.

The STROVA and COVA programmes were dedicated to the validation of the computer codes. The STROVA programme [17] consisted in applying well-defined transient loads to a variety of metal structures (representative of the reactor roof and the components of the reactor vessel) and in comparing the experimental results with those computed by the EURDYN structural dynamics code.

The COVA programme (COde VAlidation) [2, 14, 15] relied on a series of experiments performed in cylindrical tanks, starting with simple tests and increasing in complexity in such a way that only one new feature was introduced at a time. This programme aimed at validating [16, 40] the ASTARTE and SEURBNUK codes.

The WINCON and MARA programmes involved tests of gradual complexity which were based on small-scale replicas of reactors. The interest of the WINCON programme (WINfrith CONtainment) [37] consisted both in understanding the influence of the presence of each internal structure in the global response of the reactor and in validating the SEUBNUK and EURDYN codes.

Based on a 1/30 scale model of the Superphenix reactor, the French programme MARA involved ten tests of gradual complexity due to the successive addition of internal deformable structures:

- MARA 1 and 2 considered a vessel partially filled with water, with a rigid roof [1],
- MARA 4 represented the main core support structures [38],
- MARA 8 and 9 used a flexible roof [12],
- MARA 10 included the core support structures and a simplified representation of the structures above the core [23].

The French code SIRIUS [4, 10] was validated on the MARA programme [5, 24]. Like other codes using a Lagrangian approach, SIRIUS required rezoning during calculation because the deformation of the internal structures caused a great distortion of the fluid meshes. Sodium and the thick structures (the roof) were described with the Finite Difference Method while the Finite Element Method was used for the thin structures (the vessel). Argon and the bubble were not meshed but taken into account by a law computing volume versus pressure.

At the end of the 80s, it was preferred to add a specific HCDA sodium–bubble–argon tri-component constitutive law [20] to the general fast dynamics finite element CASTEM-PLEXUS code. The HCDA constitutive law was validated [8] by the CONT benchmark [3].

In order to demonstrate the capability of CASTEM-PLEXUS to predict the behaviour of real reactors [7, 21], axisymmetrical computations of the MARA series were confronted with the experimental results. The computations performed at the beginning of the 90s showed a rather good agreement between the experimental and computed results for the MARA 8 and MARA 10 tests [6]. However, numerical results showed some discrepancies which might be eliminated by increasing the fineness of the mesh. Afterwards, the CASTEM-PLEXUS code was merged with the PLEXIS-3C code to extend the capacities of both codes. The result was the EUROPLEXUS code.

To conclude the MARA 8 test, the mesh was refined and another comparison between the experimental and numerical results with a more detailed analysis of the results was undertaken. After a brief presentation of the MARA 8 mock-up and of the EUROPLEXUS code, this paper focuses on the numerical model, the analysis of the numerical results, and a comparison of the current numerical results with the experimental results and the previously computed ones.

2. Description of the MARA 8 mock-up

In France, the two Liquid Metal Fast Breeder Reactors (LMFBR) Phenix and Superphenix (see Fig. 1) are based on an integrated design: the entire primary circuit of the reactor (core, pumps, heat exchangers, etc.) is contained inside the reactor vessel. The exchanges with the secondary circuit are limited to some pipes crossing the reactor roof. The main advantage of this design is to

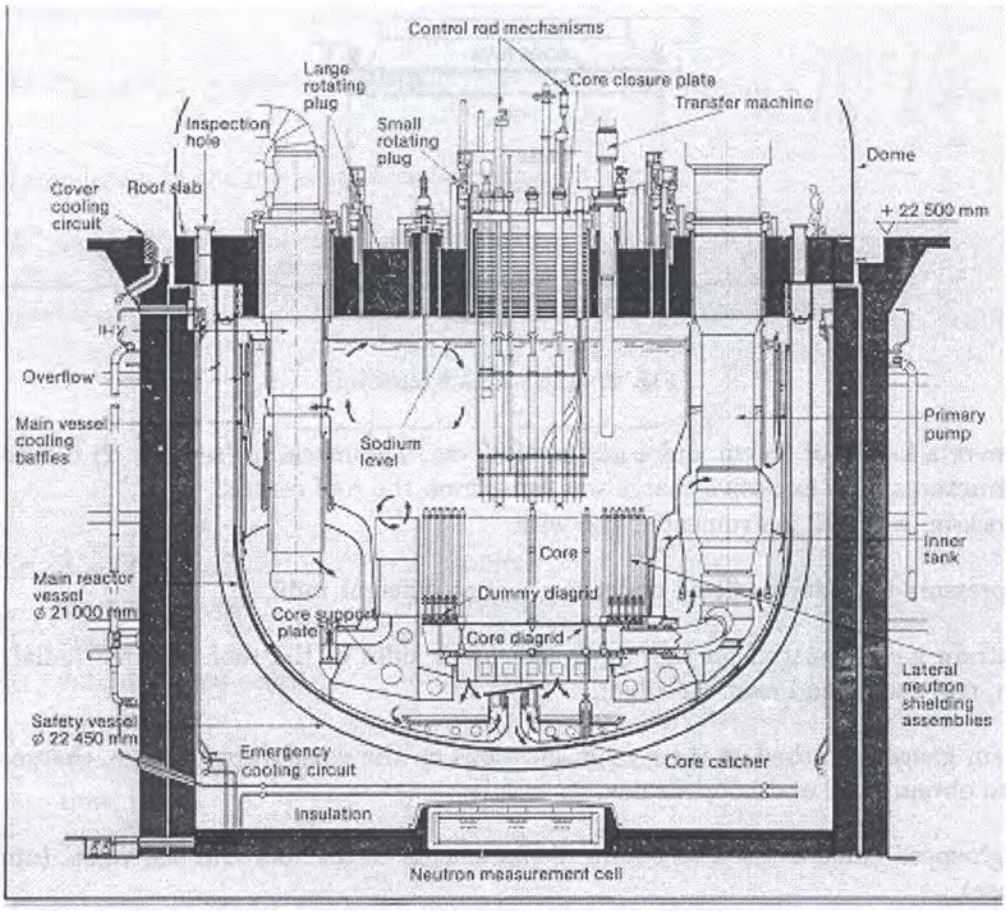

Fig. 1. The Superphenix reactor

maintain the majority of the radioactive elements inside the reactor vessel and to limit the possible contacts between air and the radioactive sodium of the primary circuit. As sodium is flammable on contact with air, a blanket of inert gas (argon) isolates the sodium in the reactor block from the reactor roof.

The MARA programme was defined and carried out at the CEA-Cadarache in the 80s in order to simulate a Hypothetical Core Disruptive Accident in simplified small-scale models of the Superphenix reactor block. The characteristics of the MARA mock-ups were [6]:

- a scale factor of 1/30 for all dimensions and thicknesses,
- an axisymmetrical geometry.

In order to carry out tests at ambient temperature and to avoid fire problems linked to sodium handling, liquid sodium was replaced by water in tests since both components have similar densities and viscosities. Argon was replaced by air, and the bubble expansion was simulated by an explosive source.

All tests of the MARA series were fired using a 45 g low-density low-pressure explosive charge of L54/16 composition [11] leading to at least a 1000 MJ full-scale energy release [24]. Vessels were filled with water, leaving a 4.3 cm air gap [12]. The vessels of all the tests were identical and made of 316 steel 1.2 mm thick. Between the junction with the core support plate and the junction with the internal heat exchangers, thickness was reduced locally to 0.9 mm and 1.1 mm in order to simulate a pinned attachment with the diagrid.

In MARA 8, a flexible roof of A42 steel 10 mm thick was clamped to the roof support [12]. The vessel was welded to a flange bolted to the roof support. The external dimensions of the MARA 8

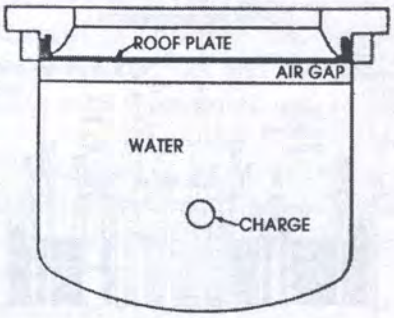

Fig. 2. The MARA 8 mock-up

mock-up were a height of 55 cm and a radius of 35 cm. The mock-up (see Fig. 2) did not include internal structures. The explosive charge was hung from the roof centre.

The mock-up was well instrumented [12] with:

- seven pressure transducers fitted under the roof at different radii,
- eight strain gauges placed on the upper and lower sides of the roof at three radial locations (centre, mid-radius and near the edge),
- six strain gauges attached at three main locations on the vessel (upper bulge, charge level and base) to obtain axial and hoop strains,
- two high-speed cameras used to obtain displacements of the roof and the vessel (upper bulge and base).

The residual deformations were evaluated by measuring, before and after the firing, the mesh sizes of the grid drawn on the vessel and the roof.

3. Description of the EUROPLEXUS computer code and of the HCDA constitutive law

EUROPLEXUS is a general computer code [9, 13, 25], co-developed by CEA-Saclay and JRC-Ispra, for the analysis of fast transient phenomena. EUROPLEXUS results from the merging of the CASTEM-PLEXUS and PLEXIS-3C codes. It can perform 1D, 2D or 3D structure calculations as required. The main fields dealt with are impacts [27], explosions [26, 28, 29, 33, 35], pipe circuits [18, 19, 30, 36], hydrodynamics [39] and robots [22].

EUROPLEXUS is based on the Finite Element Method. Time integration is explicit and the formulation can be Lagrangian, Eulerian or Arbitrary Lagrange Euler (ALE). The code can take into account various non-linearities related to materials or geometry. EUROPLEXUS calculates successively, at each time step, the mass conservation, the total energy conservation only if needed, the material constitutive law and finally the momentum conservation law.

The HCDA constitutive law of the EUROPLEXUS code supposes that the sodium–argon–bubble mixture is homogeneous in each mesh. Each constituent is described by a specific constitutive law, and it is assumed that the presence of the other constituents does not affect the constitutive law of each one. Thermal transfers between constituents during the explosion are assumed to be negligible. As a consequence of this simplification, the code does not use the energy equation for the resolution of HCDA problems.

Mass conservation is ensured by balancing the flows crossing the mesh boundary during the time step. Then the code solves the weak formulation of the momentum equation:

– Mass conservation

$$M^{(n+1)} = M^{(n)} + \Delta M^{(n \to n+1)} = M^{(n)} - \int_{t^{(n)}}^{t^{(n+1)}} \oint_A \rho\, \vec{n} \cdot \vec{v}\, \mathrm{d}A\, \mathrm{d}t + \int_{t^{(n)}}^{t^{(n+1)}} \int_V M_{\text{ext}}\, \mathrm{d}V\, \mathrm{d}t\,,$$

– Weak formulation of the momentum conservation

$$\underbrace{\int_V \vec{\mathcal{U}}^* \cdot \rho \frac{\partial \vec{v}}{\partial t}\, \mathrm{d}V\, \mathrm{d}t}_{M^{(n+1)}\,\vec{\gamma}^{(n+1)}} = \underbrace{-\int_V \vec{\mathcal{U}}^* \cdot \left(\rho\, \vec{v} \cdot \bar{\bar{\dot{\epsilon}}}\right) \mathrm{d}V\, \mathrm{d}t}_{\text{transport force}} + \underbrace{\oint_A \vec{n} \cdot \left(\vec{\mathcal{U}}^* \cdot \bar{\bar{\sigma}}\right) \mathrm{d}A\, \mathrm{d}t}_{\text{boundary conditions}}$$

$$\underbrace{-\int_V \bar{\bar{\epsilon}}^* : \bar{\bar{\sigma}}\, \mathrm{d}V\, \mathrm{d}t}_{\text{internal forces}} + \underbrace{\int_V \vec{F}_{\text{ext}}\, \mathrm{d}V\, \mathrm{d}t}_{\text{external forces}}\,,$$

with

A	bounding surface	V	volume
$\vec{F}_{\text{ext}}$	external forces	$\vec{v}$	velocity
M	mass	$\vec{\gamma}$	acceleration
M_{ext}	external mass source	ρ	density
$\vec{n}$	normal vector	$\bar{\bar{\epsilon}}^*$	strain (spatial derivative of $\vec{\mathcal{U}}^*$)
n	time step	$\bar{\bar{\dot{\epsilon}}}$	strain speed (spatial derivative of $\vec{v}$)
t	time	$\bar{\bar{\sigma}}$	stress
$\vec{\mathcal{U}}^*$	arbitrary displacement		

In the Finite Element Model, the nodal variables (velocity, acceleration, etc.) are identical for the three constituents of the HCDA law. On the contrary, the elementary variables (pressure, density, etc.) depend on several parameters: the partial variables of each constituent, the presence fraction x of constituents, etc. The quantities related to each constituent (a for argon, b for bubble, s for sodium and v for sodium vapour) are indicated with a subscript. Quantities without a subscript are related to the homogeneous mixture, and index g is related to the gas mixture.

For instance, the mixture density is obtained by

$$\rho = \rho_a\, x_a + \rho_b\, x_b + \rho_s\, x_s + \rho_v\, x_v\,.$$

The pressure of the gas mixture p_g is the sum of partial pressures,

$$p_g^{(n+1)} = p_a^{(n+1)} + p_b^{(n+1)} + p_v^{(n+1)}\,. \tag{1}$$

The void fraction α is obtained from the ratios between the relative density ϕ of a component (density related to the total volume of the mesh) and the absolute density of the component,

$$\alpha = \frac{\phi_a}{\rho_a} = \frac{\phi_b}{\rho_b} = \frac{\phi_v}{\rho_v} = \frac{\phi_g}{\rho_g} = 1 - \frac{\phi_s}{\rho_s}\,. \tag{2}$$

The fluid mixture is described by the constitutive laws of each component [21].

- Argon is assumed to be a perfect gas with an adiabatic behaviour,

$$p_a^{(n+1)} = p_a^{(n)} \left(\frac{\rho_a^{(n+1)}}{\rho_a^{(n)}} \right)^{\lambda_a} \tag{3}$$

where λ_a is the heat capacity ratio c_p/c_v.

- The bubble is considered as a perfect gas whose behaviour follows a polytropic law,

$$p_b^{(n+1)} = p_b^{(n)} \left(\frac{\rho_b^{(n+1)}}{\rho_b^{(n)}} \right)^{\eta_b}. \tag{4}$$

The exponent η_b can have any positive value. For instance, $\eta_b = 1$ for an isothermal law or $\eta_b = \lambda_b$ for an adiabatic law.

- Sodium can exist in a liquid phase and a gaseous shape because of the possibility of cavitation. The diphasic sodium is supposed to be at saturation conditions, and its temperature is assumed to be constant. The liquid is submitted to pressure

$$p_s^{(n+1)} = p_g^{(n+1)} = p_s^{(n)} + C_s^2 \left(\rho_s^{(n+1)} - \rho_s^{(n)} \right) \tag{5}$$

with C_s the sound velocity in sodium. The vapour only depends on the initial temperature $T^{(0)}$,

$$p_v^{(n+1)} = p_{\text{sat}} \left(T^{(0)} \right).$$

EUROPLEXUS computes the average density and the concentration of each constituent from the mass conservation for each fraction. Then the pressure of the mixture is obtained by successive iterations. The iterative process computes:

1. The sodium density from (5) by estimating approximately $p_s^{(n+1)}$ at the beginning of the time step,
2. The void fraction and then the argon and bubble densities from (2),
3. The argon pressure from (3),
4. The bubble pressure from (4),
5. The mixture pressure from (1).

4. Numerical modeling of the mock-up

The MARA 8 mock-up is composed of structures and fluids interacting with each other. The mock-up includes a flexible vessel with a flexible roof. Structures are assumed to be thin and flexible enough to be represented by shells.

In the case of a HCDA, the internal fluids are sodium, argon and a gas bubble. In the test, these fluids are respectively replaced by water, air and an explosive charge. Water and air are initially at atmospheric pressure, whereas the explosive charge induces an initial pressure of 165 MPa in the bubble area. The characteristics included in the numerical model are:

- Water: $\rho = 998.3$ kg/m^3; sound speed $C = 1550$ m/s; $p^{(0)} = 10^5$ Pa; $\rho_{\text{sat}} = 0.0172$ kg/m^3; $p_{\text{sat}} = 2337$ Pa
- Air: $\rho = 1.206$ kg/m^3; $\lambda = c_p/c_v = 1.4$; $p^{(0)} = 10^5$ Pa
- Explosive charge: $\rho = 400$ kg/m^3; polytropic coef. $\eta = \lambda = 1.24$; $p^{(0)} = 1.646 \cdot 10^8$ Pa.

In this study, fluid–structure coupling is realised by defining coupling elements between solid elements and fluid elements. Thanks to coupling elements, the fluid nodes and solid nodes at the interface have the same displacements. The main drawback of this method comes from the absence

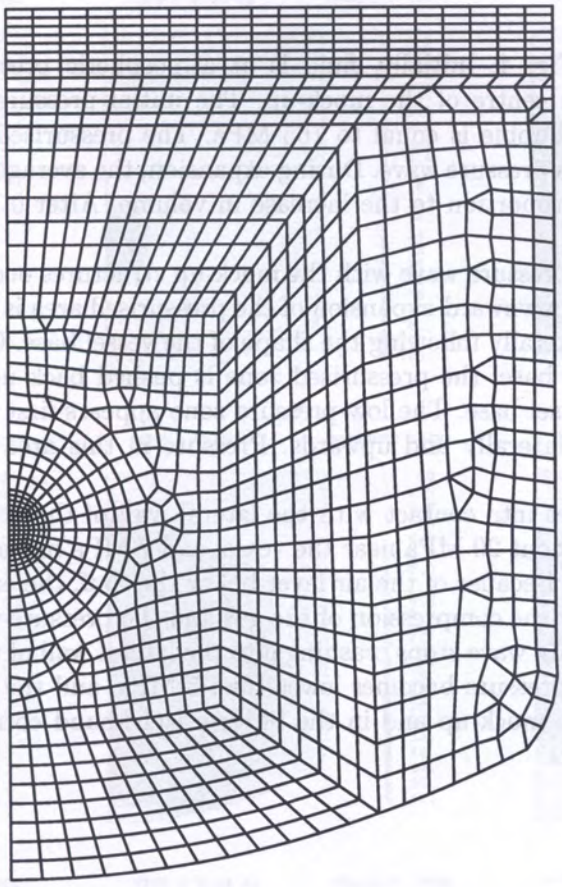

Fig. 3. Mesh of the MARA 8 test

of automatic actualisation of the ALE grid for the elements other than the ones along the coupling lines.

This coupling has been adopted for the MARA 8 test because the geometry is sufficiently simple to define coupling elements easily and because no huge distortion of the fluid mesh is expected. Owing to the symmetry of the mock-up, an axisymmetrical representation (see Fig. 3) is used for the numerical simulation.

Boundary conditions are:

- No horizontal displacement on the symmetry axis,
- No rotation of the two vessel and roof nodes located on the symmetry axis,
- Complete blocking of the node in the top corner at the junction between the vessel and the roof.

5. Results

The interpretation of the numerical results [31, 34] is based on the analysis of pressure, gas fraction, fluid speed, radial and vertical displacements, stresses and strains versus time. The evolution of these variables is presented in images showing the state of internal fluids or structures at different times.

5.1. Pressure

Pressure is presented in Fig. 4. Initially, fluid is at atmospheric pressure, apart from the high pressure gas bubble in the centre of the mock-up. The initial pressure induced by the explosive charge simulating the gas bubble is equal to 165 MPa. The pressurised zone expands spherically, causing the propagation of a pressure wave. During expansion, the average pressure of the pressurised zone decreases in inverse proportion to the increase in volume. After 0.1 ms, pressure in this zone goes down to 30 MPa.

The first contact of the pressure wave with the mock-up structures occurs at the vessel base after 0.14 ms. Consequently the downward expansion of the pressurised area is stopped by the vessel base, and expansion continues laterally following the shape of the vessel base. Owing to the pressure wave rebound against the vessel base, the pressurised zone is pushed back upwards and a low-pressure zone appears above the vessel base. The low-pressure zone appears first next to the symmetry axis and spreads progressively laterally and upwards. Pressure in this area is approximately equal to atmospheric pressure.

The pressure wave comes into contact with the lateral wall of the vessel after 0.22 ms. At that time, pressure is equal to about 20 MPa near the vessel and 7 MPa in the initial pressurised zone in the middle of the mock-up. Because of the air layer below the roof, the excess pressure at the top of the mock-up is absorbed by the compression of the gas and the pressure wave does not bounce back against the roof. The pressure wave stops crashing into the lateral wall of the vessel at approximately 0.35 ms. Afterwards, fluid pressure becomes lower than 5 MPa, and the most pressurised areas are located in the centre of the mock-up and in the bottom right-hand corner adjoining the base and the lateral wall of the vessel.

5.2. Gas fraction

Figure 5 illustrates the evolution of the volumic presence fraction of gas. In order to interpret correctly the presence of each constituent, the massic presence fractions of the bubble and air are described in Figs. 6 and 7. Initially, the gas is located in the middle of the mock-up (bubble) and below the roof (air).

The expansion of the gas bubble starts immediately: a diphasic layer composed of liquid water and bubble gas appears around the initial bubble location from 0.02 ms. Then the bubble bag expands spherically. During the expansion phase of the pressure wave, the water remains liquid since the local high pressure prevents vaporisation.

From 0.3 to 1.5 ms, the bubble expands spherically and moves away from the mock-up centre. Due to the progressive emptying of the mock-up centre, depressurisation in and around the initial bubble location is observed. After the passing of the pressure wave, the water vaporises slightly and steam trails in the depressurised areas are observed:

- above the vessel base at about 0.3 ms,
- roughly between mid-radius and the lateral wall and below the air layer from 0.5 to 1.5 ms.

From 1.5 to 3 ms, the bubble gas goes on expanding but starts shifting slightly upwards as the vessel base limits the downward expansion. Steam condenses so that the gas bubble becomes surrounded only by liquid water. Between 3 and 5 ms, the bubble expands laterally to some extent but mainly vertically. After 5 ms, as the upward progression is limited by the presence of the roof, the bubble spreads laterally again. Between 5 and 7 ms, a gaseous layer above the vessel base appears; it may be composed of steam.

The air layer remains unchanged as long as the shock wave does not reach the top area. From 0.2 ms, the bottom of the air layer begins to be compressed upwards near the symmetry axis. Progressively, the entire layer is compressed and pushed towards the top right-hand corner. At about 4 ms, the air is completely flattened into the top corner, and the size of the air bag has

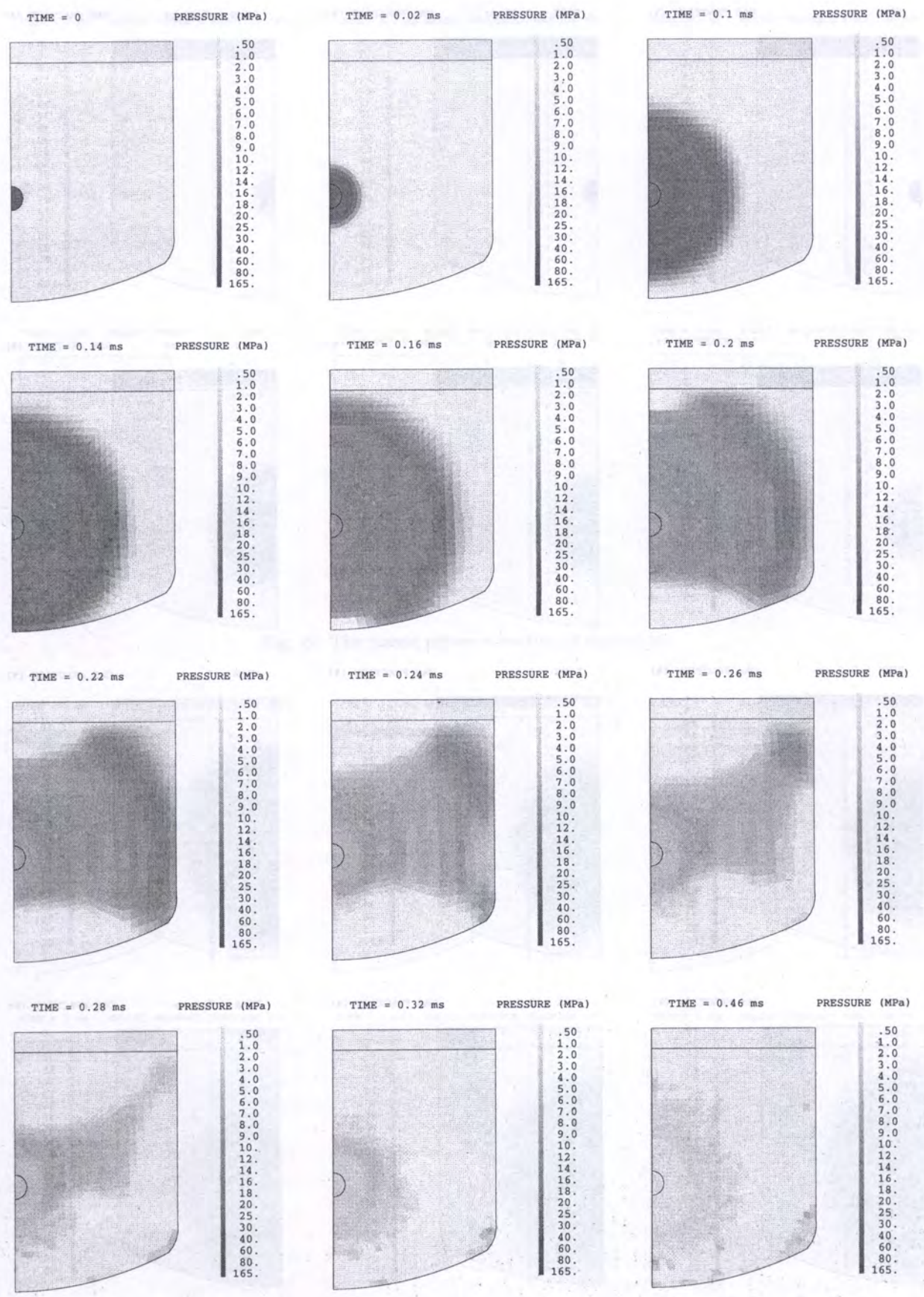

Fig. 4. Pressure

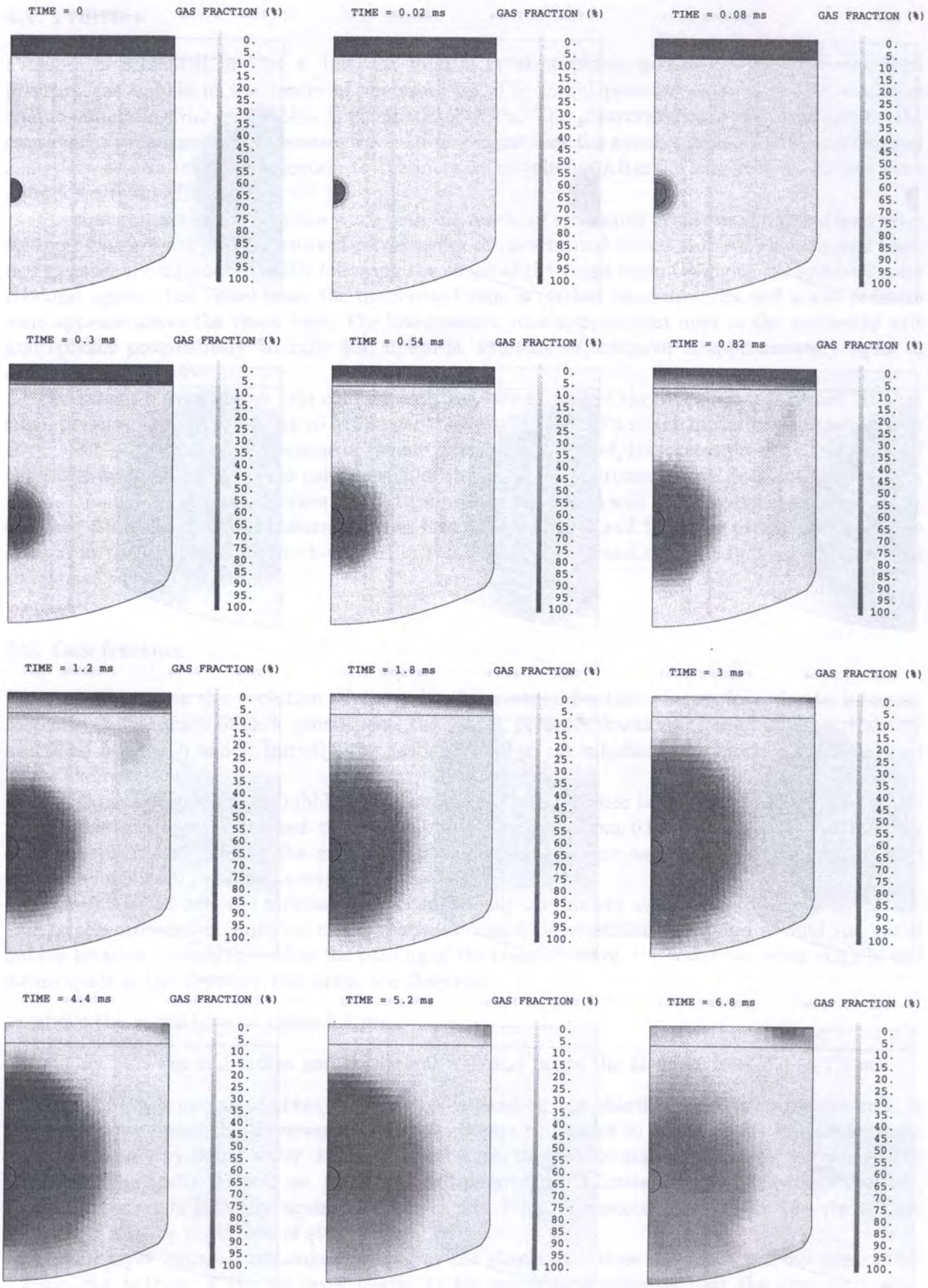

Fig. 5. The volumic presence fraction of gas

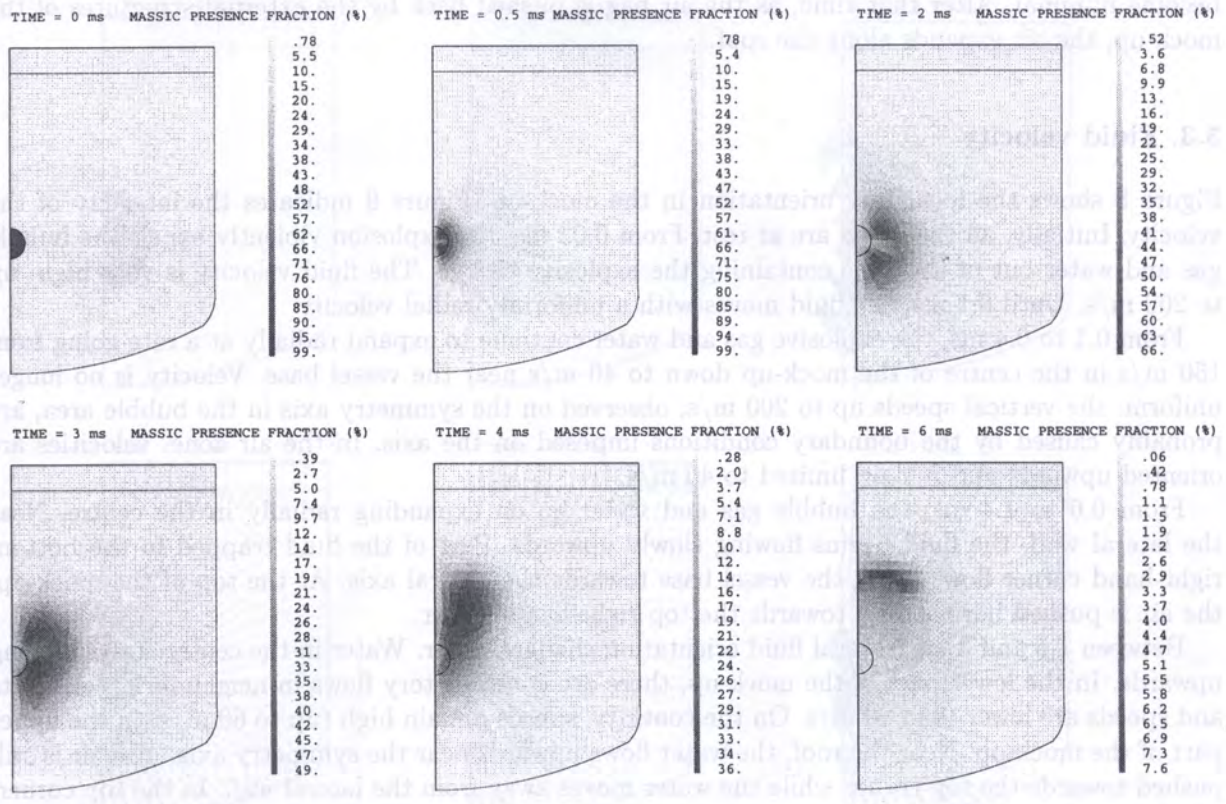

Fig. 6. The massic presence fraction of the bubble

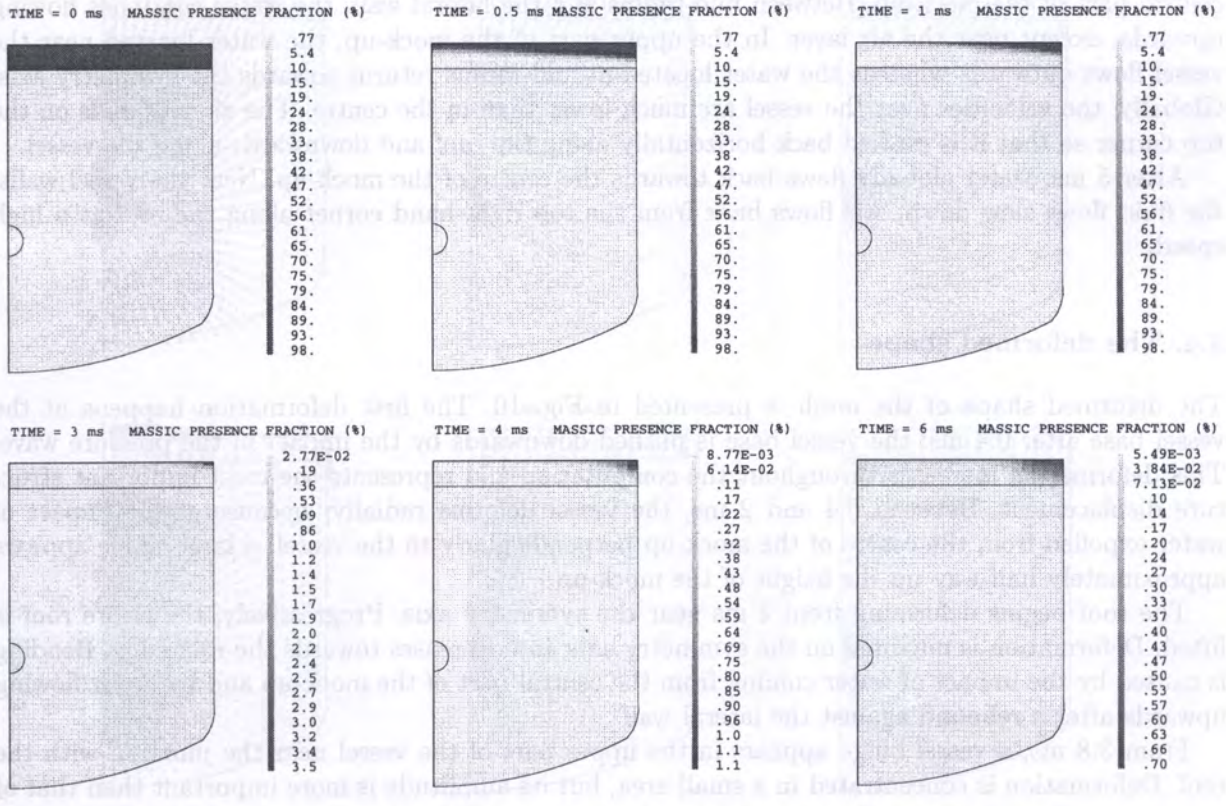

Fig. 7. The massic presence fraction of air

become minimal. After that time, as the air bag is pushed back by the external structures of the mock-up, the air expands along the roof.

5.3. Fluid velocity

Figure 8 shows the local flow orientation in the mock-up. Figure 9 indicates the intensity of the velocity. Initially, all the fluids are at rest. From 0.02 ms, the explosion violently expels the bubble gas and water out of the zone containing the explosive charge. The fluid velocity is very high: up to 200 m/s. Until 0.1 ms, the fluid moves with a uniformly radial velocity.

From 0.1 to 0.4 ms, the explosive gas and water continue to expand radially at a rate going from 150 m/s in the centre of the mock-up down to 40 m/s near the vessel base. Velocity is no longer uniform: the vertical speeds up to 200 m/s, observed on the symmetry axis in the bubble area, are probably caused by the boundary conditions imposed on the axis. In the air zone, velocities are oriented upwards and remain limited to 40 m/s.

From 0.6 to 1.4 ms, the bubble gas and water go on expanding radially in the centre. Near the lateral wall, the fluid begins flowing slowly upwards. Part of the fluid trapped in the bottom right-hand corner flows along the vessel base towards the central axis. At the top of the mock-up, the air is pushed horizontally towards the top right-hand corner.

Between 1.5 and 3 ms, several fluid orientation changes occur. Water in the centre starts moving upwards. In the lower part of the mock-up, there are contradictory flows in neighbouring elements and speeds are lower than 20 m/s. On the contrary, speeds remain high (up to 60 m/s) in the upper part of the mock-up. Near the roof, the water flows upwards near the symmetry axis. The air is still pushed towards the top corner while the water moves away from the lateral wall. In the top corner, the air speed reaches locally 200 m/s.

Between 3 and 5 ms, high speeds (up to 150 m/s) are reached due to the general rebound of the fluid against the vessel. Water along the base and in the bottom right-hand corner flows back to the central part of the mock-up. Between mid-radius and the lateral wall, the water continues flowing upwards, except near the air layer. In the upper part of the mock-up, the water located near the vessel flows outwards whereas the water located at mid-radius returns towards the symmetry axis. Globally, the velocities near the vessel are much lower than in the centre. The air rebounds on the top corner so that it is pushed back horizontally along the roof and downwards along the vessel.

After 5 ms, water globally flows back towards the centre of the mock-up. Near the vessel walls, the fluid flows slow down. Air flows back from the top right-hand corner along the roof at a high speed.

5.4. The deformed shape

The deformed shape of the mesh is presented in Fig. 10. The first deformation happens at the vessel base after 0.4 ms: the vessel base is pushed downwards by the impact of the pressure wave. This deformation increases throughout the computation and represents the most important structure displacement. Between 0.4 and 2 ms, the vessel deforms radially: because of the impact of water expelled from the centre of the mock-up perpendicularly to the vessel, a large bulge appears approximately half-way up the height of the mock-up.

The roof begins deforming from 2 ms near the symmetry axis. Progressively, the entire roof is lifted. Deformation is maximal on the symmetry axis and decreases towards the roof edge. Bending is caused by the impact of water coming from the central part of the mock-up and by water flowing upwards after a rebound against the lateral wall.

From 3.8 ms, a vessel bulge appears in the upper part of the vessel near the junction with the roof. Deformation is concentrated in a small area, but its amplitude is more important than that of the previous lateral bulge. This second vessel bulge is caused by the compression of air in the top right-hand corner.

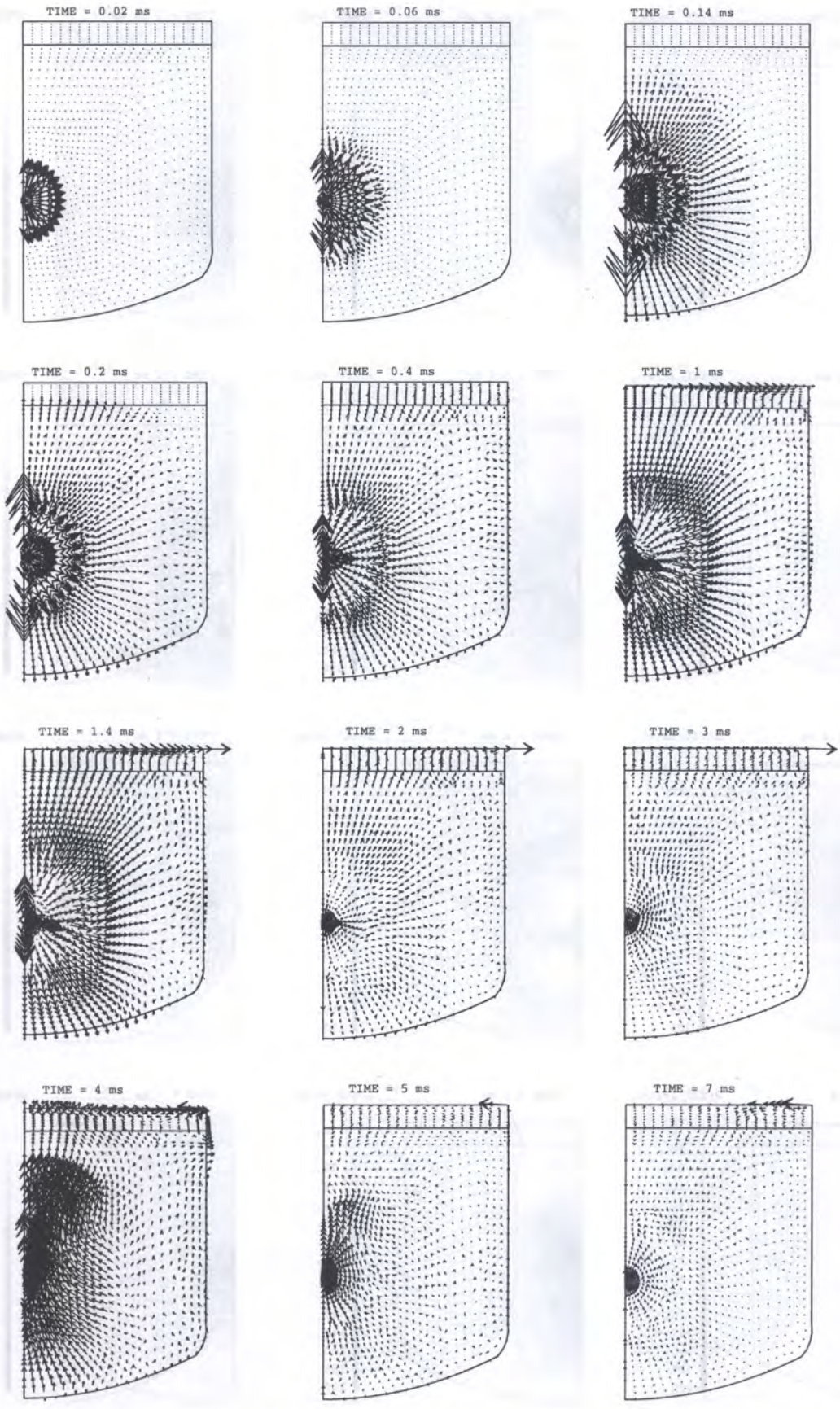

Fig. 8. Fluid speed

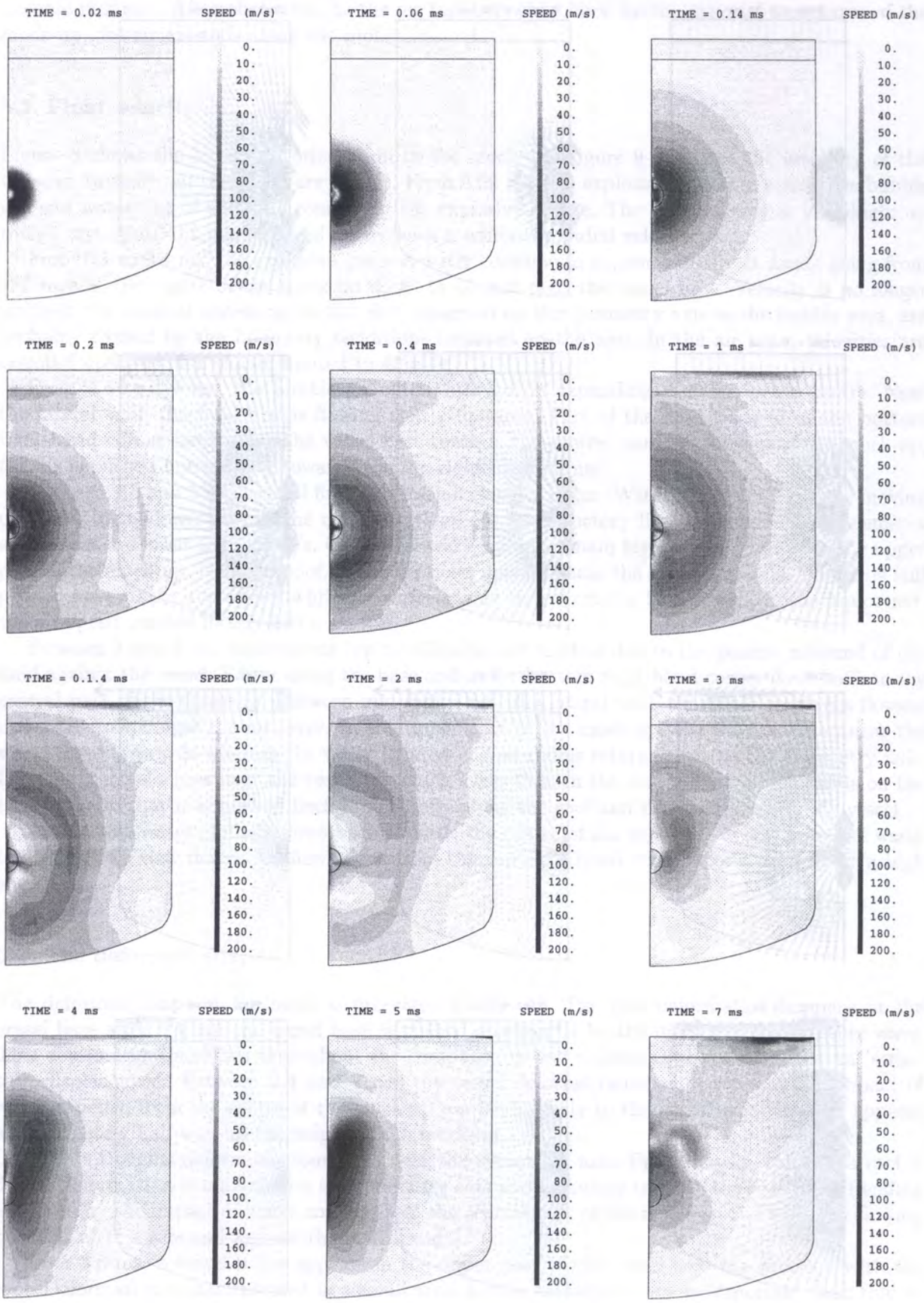

Fig. 9. Fluid speed

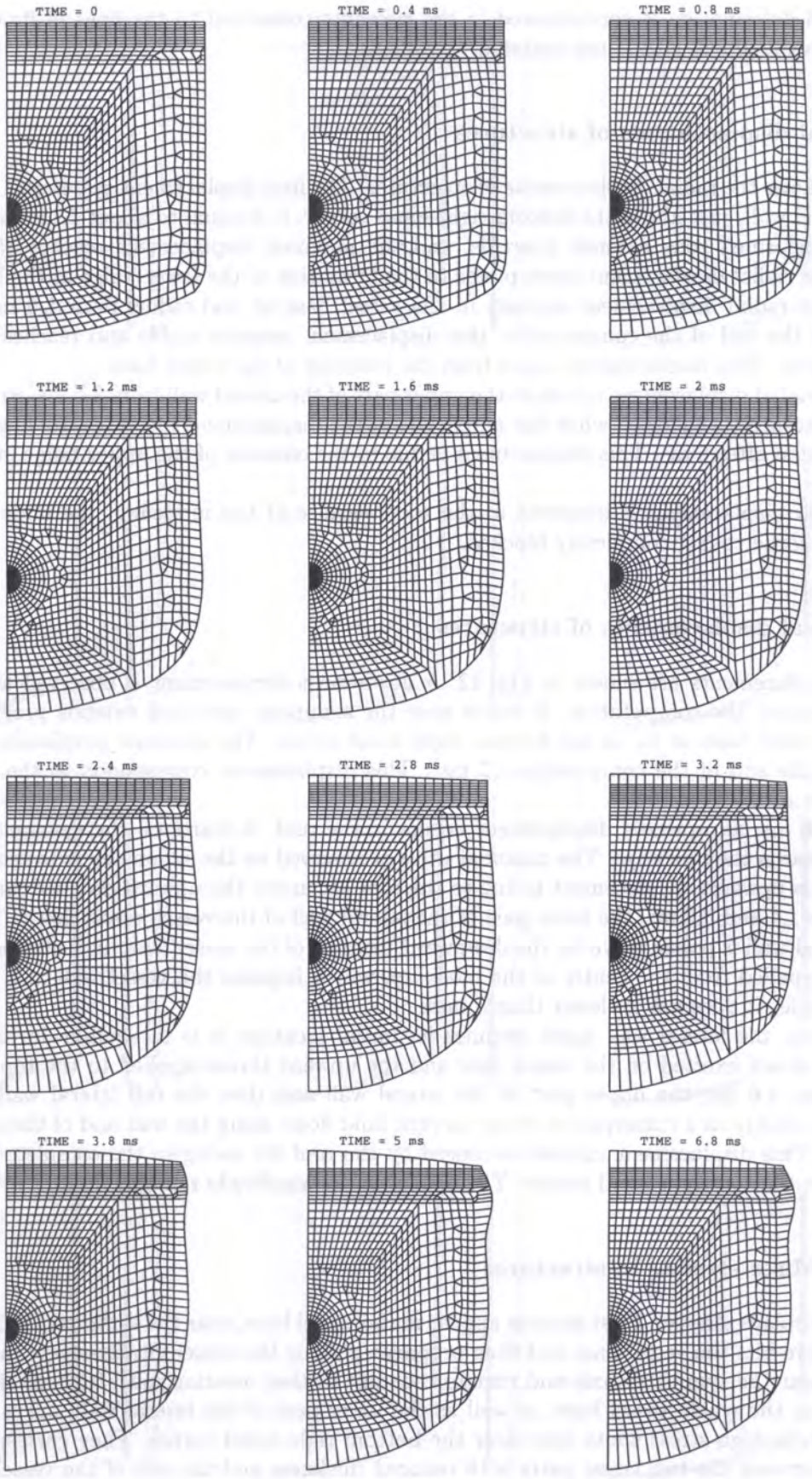

Fig. 10. The deformed shape

The grid deformation is concentrated in the elements connected to the lines of fluid–structure coupling, as the global grid is not updated.

5.5. Radial displacements of structures

Figure 11 shows the radial displacements of structures. The first displacement appears at the bottom of the lateral wall, just above the bottom right-hand corner: it is equal to about 5 mm after 0.6 ms. Then the deformed zone extends upwards, and the maximal displacement reaches 15 mm after 2.2 ms. This radial displacement corresponds to the formation of the lower bulge in the lateral wall.

A second radial displacement appears in the vessel base at mid-radius from 1.6 ms. Between 2.2 ms and the end of the computation, this displacement remains stable and reaches a maximal value of 7 mm. This displacement comes from the lowering of the vessel base.

A third radial displacement occurs in the upper part of the lateral wall from 3.6 ms. Progressively, the deformed area is enlarged while the amplitude of the displacement increases. Its maximal value reaches 20 mm after 5 ms. This displacement is due to the creation of the upper bulge in the lateral wall.

No radial displacement is observed in the roof because of the modeling, the node in the top right-hand corner being completely blocked.

5.6. Vertical displacements of structures

Vertical displacements are shown in Fig. 12. A downwards displacement is observed at the vessel base throughout the computation. It starts near the symmetry axis and extends progressively to the whole vessel base as far as the bottom right-hand corner. The maximal amplitude is equal to 55 mm at the end of the computation (7 ms). This displacement corresponds to the downwards deformation of the vessel base.

From 2.6 ms, an upwards displacement occurs in the roof. It starts on the symmetry axis and extends towards the roof edge. The maximal value is observed on the symmetry axis and is equal to 30 mm. This upwards displacement is due to the roof lift under the upward-directed water thrust.

Between 1.4 and 3.2 ms, the lower part of the lateral wall of the vessel moves down. The bottom of the lateral wall is pulled down by the downward bending of the vessel base. It is also pushed down by water expelled from the centre of the mock-up, which impacts the vessel wall at a downward-oriented angle. It does not go lower than 5 mm.

At 3.8 ms, the lateral wall again resumes its initial location: it is in equilibrium between the downward thrust exerted on the vessel base and the upward thrust applied to the top right-hand corner. From 4.6 ms, the upper part of the lateral wall and then the full lateral wall are pulled upwards, probably as a consequence of the upward fluid flows along the wall and of the upper bulge formation. This displacement cannot be caused by the roof lift owing to the complete blocking of the point in the top right-hand corner. The displacement amplitude remains limited to 5 mm.

5.7. Von Mises stresses in structures

Figure 13 displays stresses. First stresses appear in the vessel base, near the symmetry axis, when the pressure wave hits the vessel base and then propagates along the vessel. Stresses very quickly reach 500 MPa near the symmetry axis and remain constant at that location until 0.32 ms. Between 0.2 and 0.26 ms, the whole vessel base, as well as the lower part of the lateral wall, are submitted to stresses. Three high-stress spots exist near the bottom right-hand corner. They correspond to the junctions between the two vessel parts with reduced thickness and the rest of the vessel.

Between 0.32 ms and 0.4 ms, if the stresses decrease slightly in the vessel base, they increase in the lateral wall and concentrate in the bottom right-hand corner. From 0.4 to 2.4 ms, the stresses

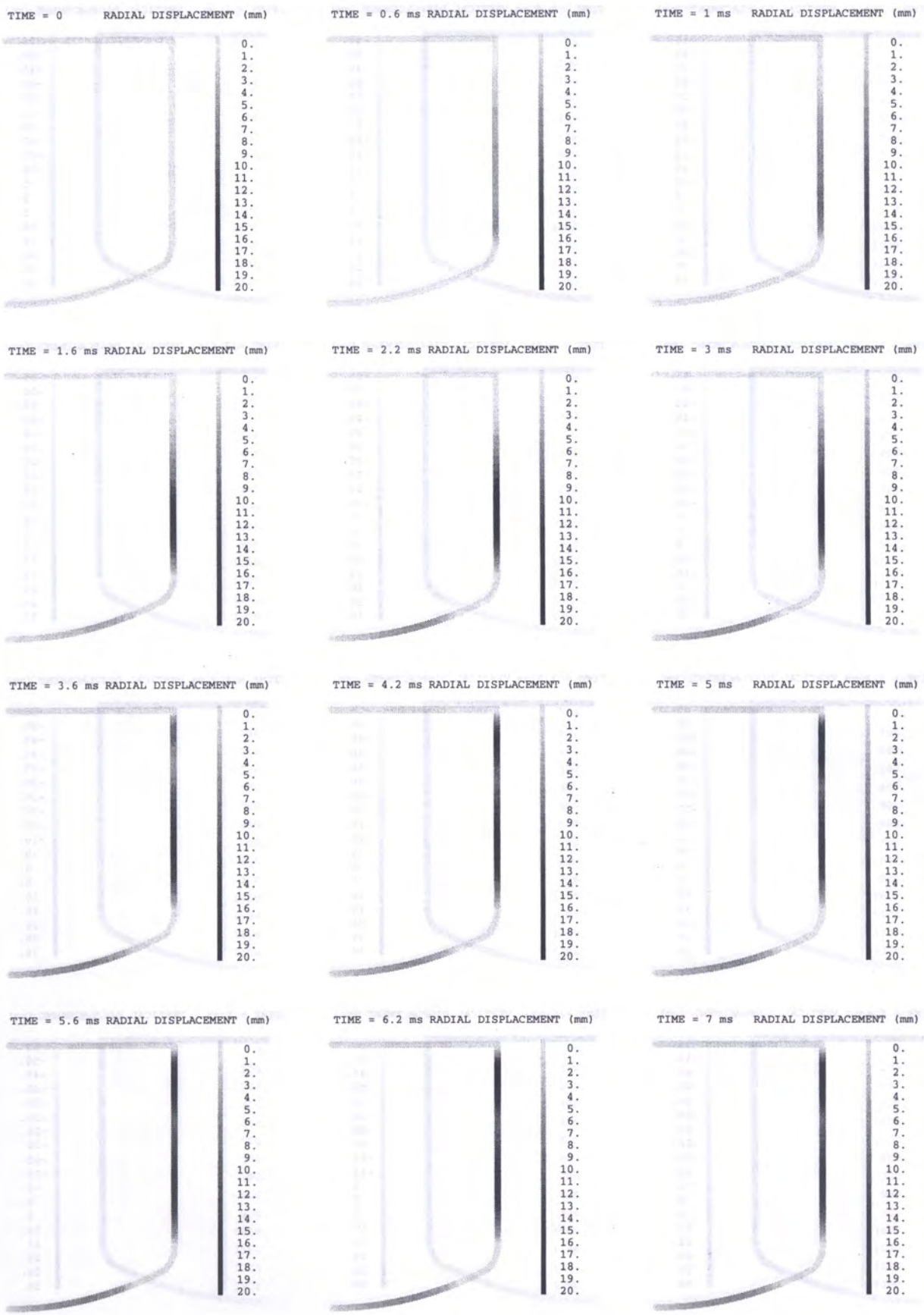

Fig. 11. Radial displacements of structures

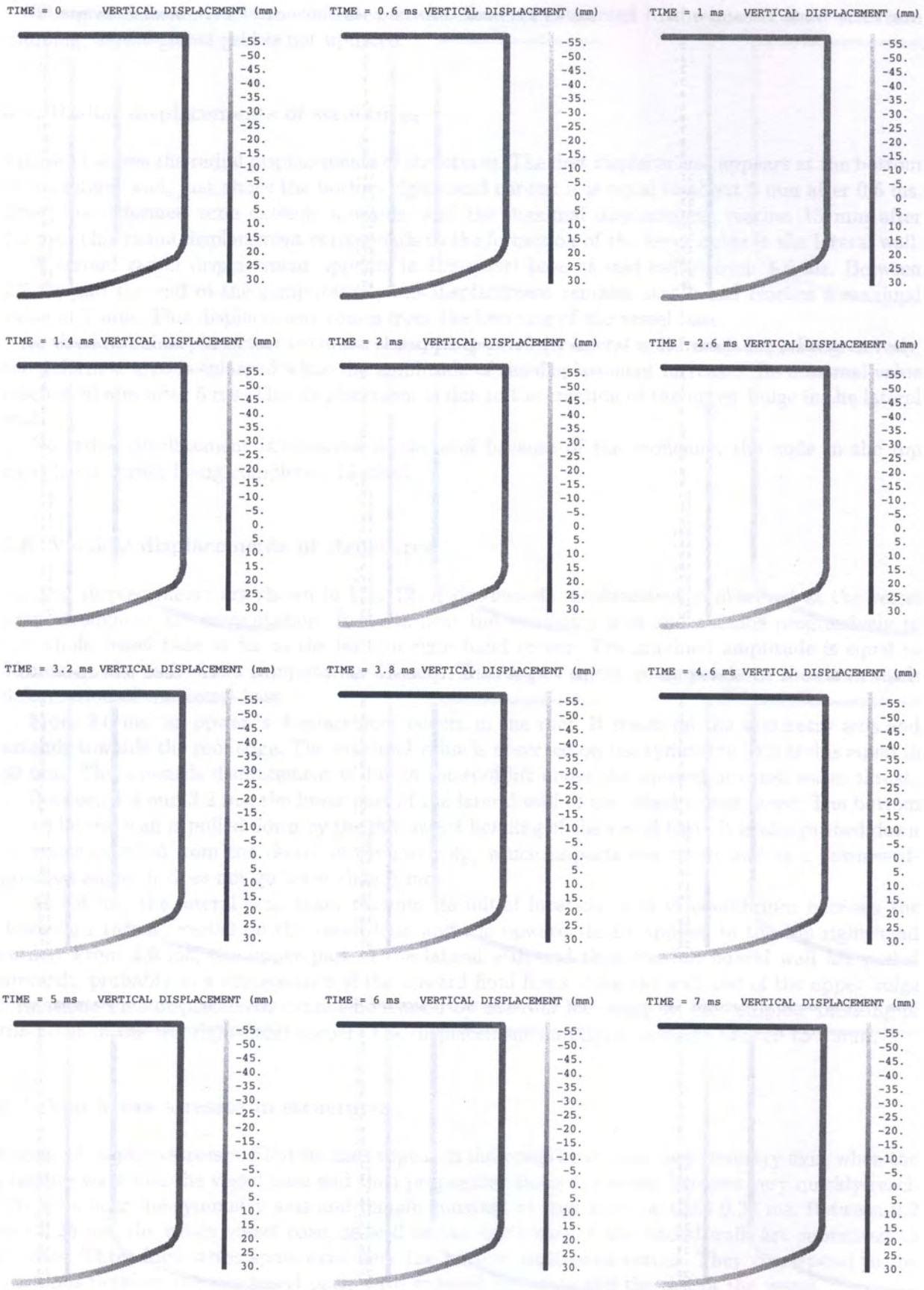

Fig. 12. Vertical displacements of structures

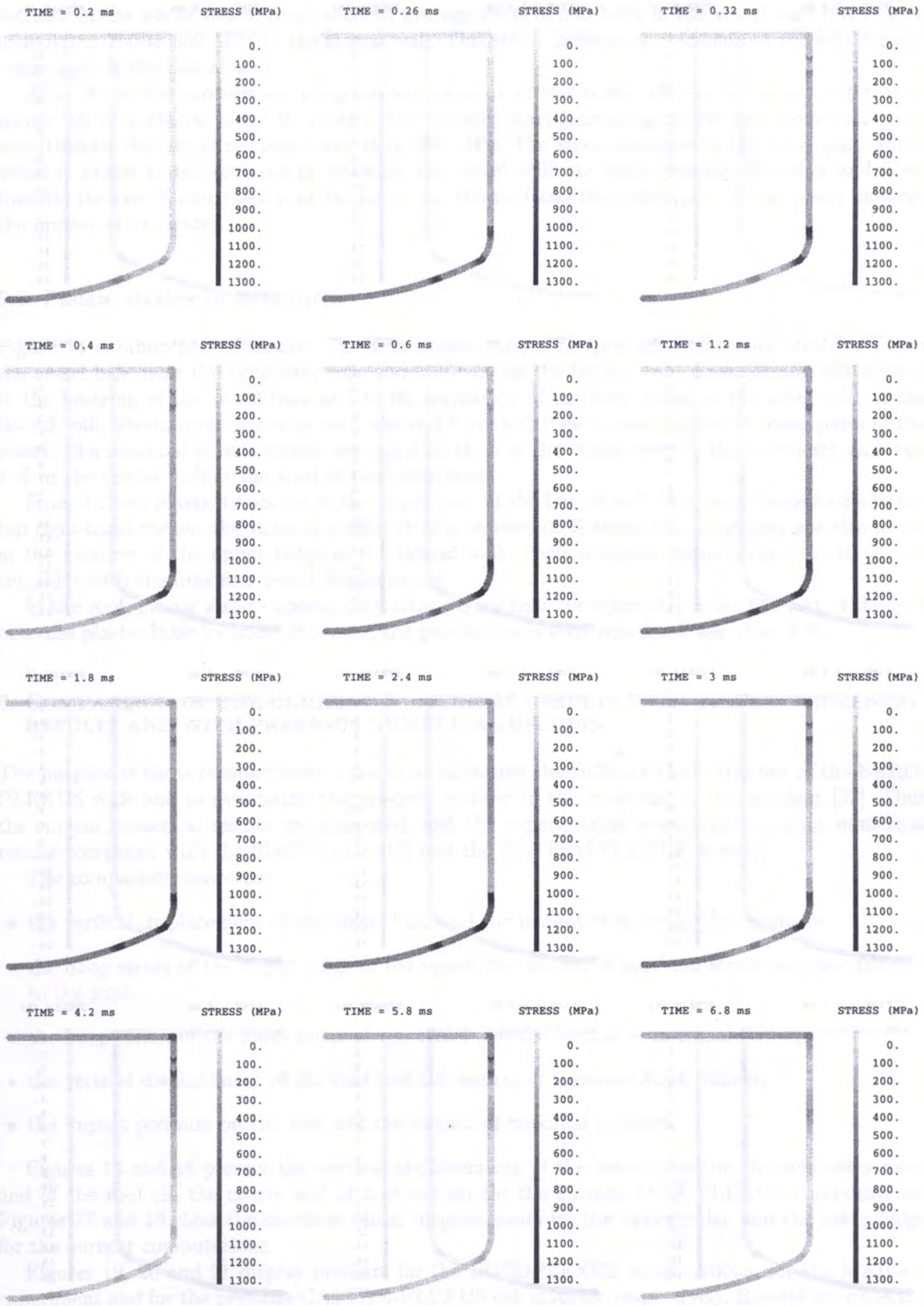

Fig. 13. Von Mises stresses

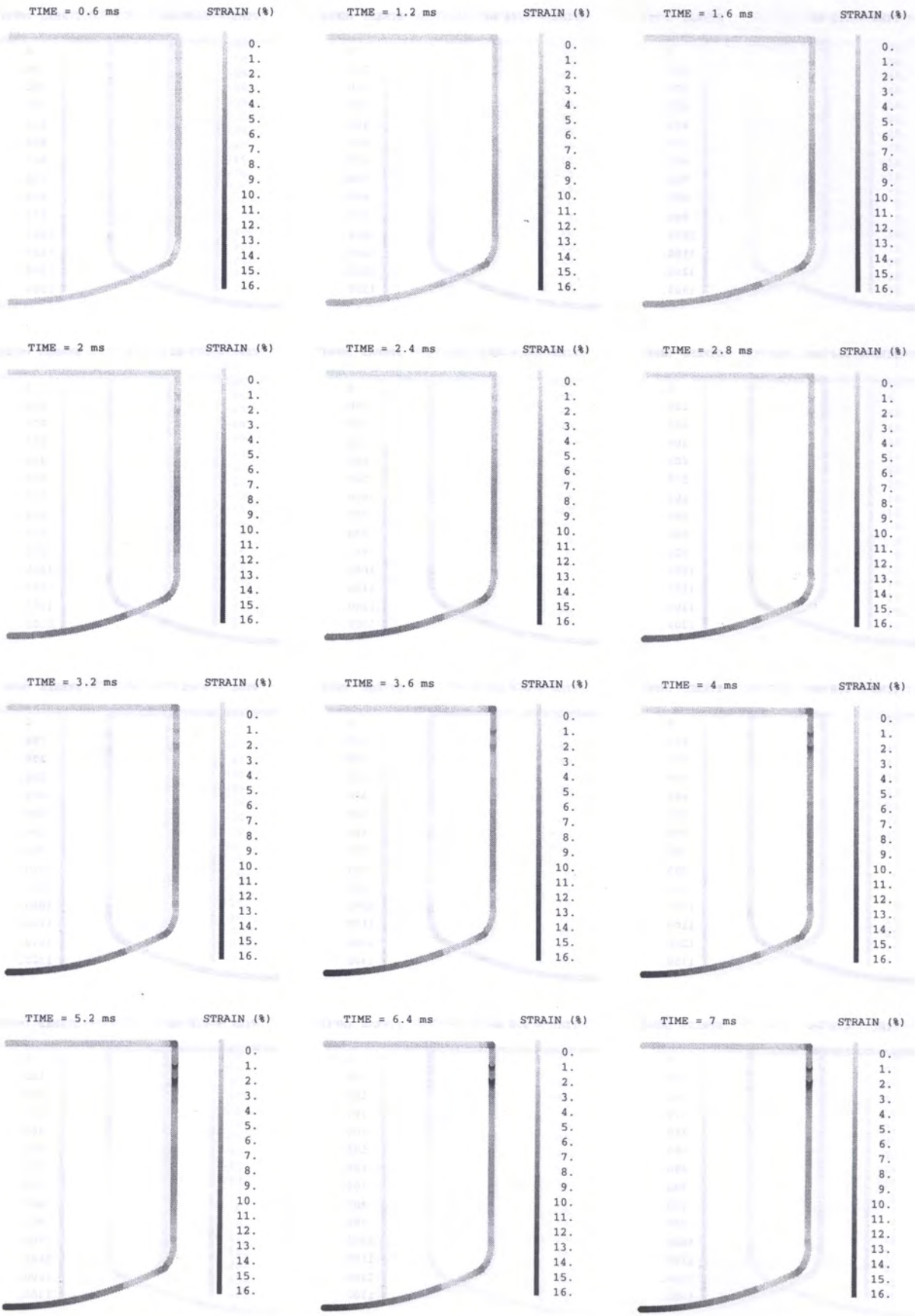

Fig. 14. Plastic strains

increase in the whole vessel: they reach an average value of 500 MPa in the vessel base but remain included in 200 to 300 MPa in the lateral wall. This stress increase corresponds to the splashing of water against the lateral wall.

After 3 ms, the stresses are progressively reduced in the vessel, except in the top right-hand corner where a plastic hinge is created. The stresses start increasing in the roof from that time; nevertheless, their level remains lower than 300 MPa. The stress decrease in the lower part of the vessel is linked to the rebound of water on the vessel wall. As water changes direction and flows towards the centre and the top of the mock-up, the roof and the upper part of the vessel undergo the impact of the water.

5.8. Plastic strains in structures

Figure 14 exhibits plastic strains. The first plastic strains happen simultaneously after 0.6 ms in the vessel base near the symmetry axis and half-way up the lateral wall. These strains correspond to the lowering of the vessel base and to the formation of the large bulge in the lower part of the lateral wall. Strain level increases until about 3.6 ms and then remains stable in these parts of the vessel. The maximal plastic strains are equal to 16 % in the vessel base on the symmetry axis and 6 % in the lateral wall at the level of the lower bulge.

From 3.2 ms, plasticity occurs in the upper part of the lateral wall. A plastic hinge forms in the top right-hand corner: the value of plastic strains reaches 10 % there. Plastic strains are also noted at the location of the upper bulge in the lateral wall. Their maximal value is equal to 16 % and coincides with the maximal vessel displacement.

In the roof, plastic strains appear only after 4.6 ms near the symmetry axis. The rest of the roof becomes plastic little by little. However, the plastic strain level remains lower than 2 %.

6. Comparison of the current numerical results with the experimental results and with previous numerical results

The purpose of these computations consists in validating the HCDA constitutive law of the EUROPLEXUS code and in estimating the progress realised in the modeling of the accident [32]. Thus the current numerical results are compared with the experimental results and previous numerical results computed with the SIRIUS code [12] and the CASTEM-PLEXUS code [6].

The comparison concerns:

- the vertical displacement of the vessel base and the instant of maximal displacement,
- the hoop strain of the upper bulge of the vessel, the instant of maximal strain and the distance to the roof,
- the hoop strain of the lower bulge of the vessel and the instant of maximal strain,
- the vertical displacement of the roof and the instant of maximal displacement,
- the impact pressure on the roof and the instant of maximal pressure.

Figures 15 and 16 present the vertical displacements of the vessel base (on the symmetry axis) and of the roof (in the centre and at mid-radius) for the current EUROPLEXUS computations. Figures 17 and 18 show the maximal radial displacements for the upper bulge and the lower bulge for the current computations.

Figures 19, 20 and 21 display pressure for the EUROPLEXUS computations, for the MARA 8 experiment and for the previous CASTEM-PLEXUS calculations, respectively. Results are collected in Table 1. The CASTEM-PLEXUS and EUROPLEXUS computations are noted CP and EP in this table.

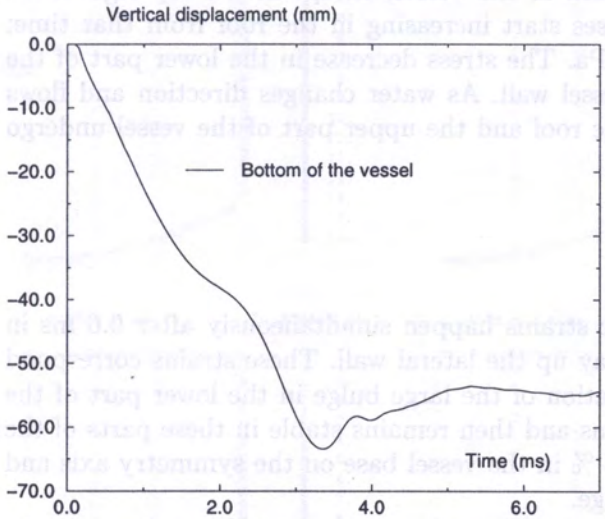

Fig. 15. Vertical displacement at the bottom of the vessel

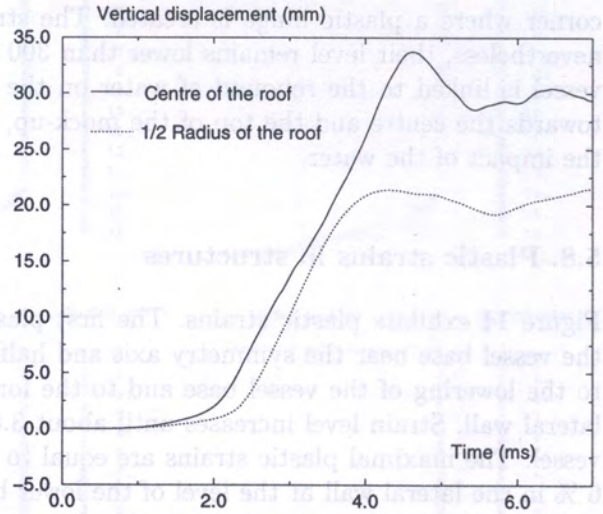

Fig. 16. Vertical displacement of the roof

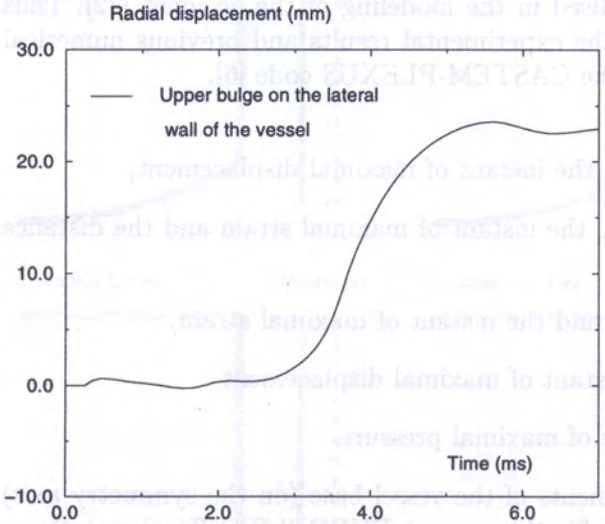

Fig. 17. Radial displacement of the upper bulge (lateral wall of the vessel)

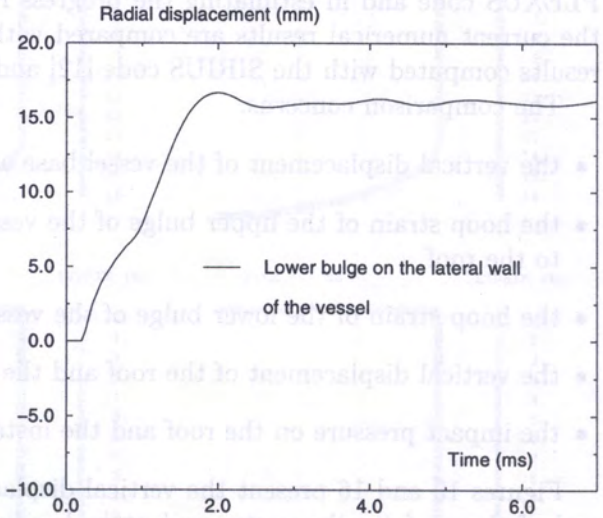

Fig. 18. Radial displacement of the lower bulge (lateral wall of the vessel)

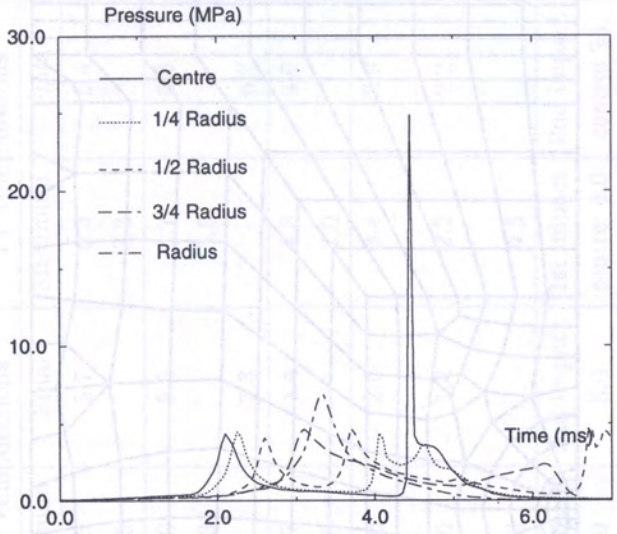

Fig. 19. Pressure under the roof

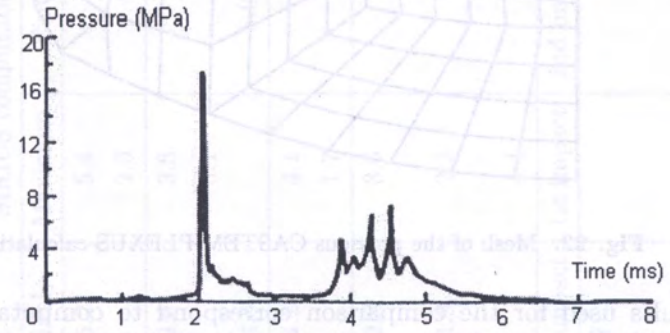

Fig. 20. Experimental pressure

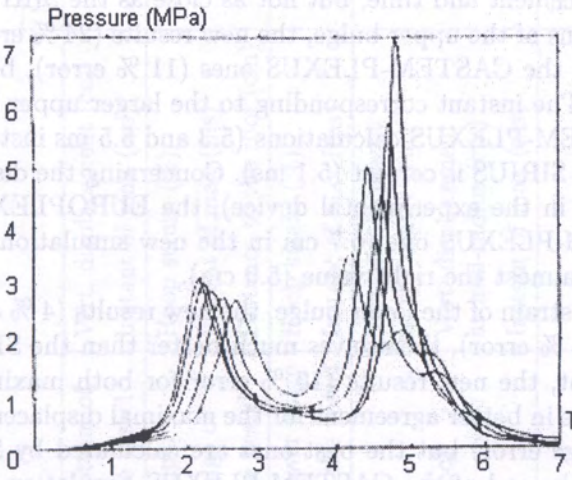

Fig. 21. Pressure under the roof, previously computed by CASTEM-PLEXUS

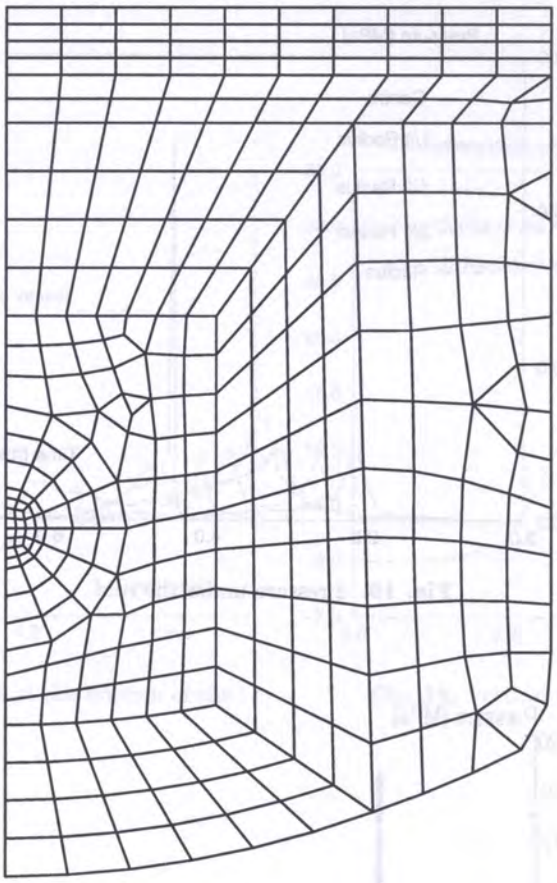

Fig. 22. Mesh of the previous CASTEM-PLEXUS calculations

The SIRIUS results used for the comparison correspond to computations based on dynamic strain–stress curves [12]. The main differences between the EUROPLEXUS and CASTEM-PLEXUS computations come from the fineness of the mesh and improvements in the treatment of fluid–structure coupling. Figure 22 presents the mesh used in the CASTEM-PLEXUS simulation.

The results in Table 1 show that, concerning the vessel base, the EUROPLEXUS results (14 % error for the maximal vertical displacement) are in closer agreement than the CASTEM-PLEXUS ones (18 % error) for displacement and time, but not as close as the SIRIUS ones (2 % error).

Regarding the hoop strains of the upper bulge, the new results (24 % error for the maximal hoop strain) are less precise than the CASTEM-PLEXUS ones (11 % error), but more precise than the SIRIUS ones (30 % error). The instant corresponding to the larger upper bulge is a bit late for the EUROPLEXUS and CASTEM-PLEXUS calculations (5.3 and 5.5 ms instead of 5.0 ms in the test) while the time computed by SIRIUS is correct (5.1 ms). Concerning the distance between the upper bulge and the roof (4.8 cm in the experimental device), the EUROPLEXUS model is a bit more accurate than the CASTEM-PLEXUS one (6.7 cm in the new simulation instead of 7.3 cm in the old one), but SIRIUS finds almost the right value (5.0 cm).

Concerning the maximal strain of the lower bulge, the new results (4 % error) are better than the CASTEM-PLEXUS ones (6 % error), themselves much better than the SIRIUS ones (18 % error).

For the roof displacement, the new results (10 % error for both maximal displacements in the centre and at mid-radius) are in better agreement for the maximal displacement than the CASTEM-PLEXUS ones (20 % average error) but the best ones are calculated by SIRIUS (5 % error). The displacement computed at the end of the CASTEM-PLEXUS simulation is better than the recent results. This difference might be lessened if the computation were carried out for a longer time. The three codes find exactly the time of the maximal displacement.

Table 1. Comparison between the experimental results and the results computed by SIRIUS, CASTEM-PLEXUS and EUROPLEXUS

		Experiment		SIRIUS computations		CP computations		EP computations	
		Maximum	Final	Maximum	Final	Maximum	Final	Maximum	Final
Bottom of the vessel	Vert. displacement (cm)	5.5	5.2	5.4		6.5	5.7	6.3	5.4
	Instant of max (ms)	2.75		2.6		3.5		3.3	
Upper bulge of the vessel	Hoop strain (%)	5.4	4.6	3.8		6.0	5.5	6.7	6.5
	Instant of max (ms)	5.0		5.1		5.3		5.5	
	Distance to the roof (cm)		4.8		5.0		7.3		6.7
Lower bulge of the vessel	Hoop strain (%)	5.0	4.2	4.1		4.7	4.4	4.8	4.6
	Instant of max (ms)	1.7		1.7		2.0		2.0	
Roof	Vert. displacement at the centre (cm)	3.8	2.8	3.6		3.0	2.6	3.4	2.9
	Vert. displacement at mid-radius (cm)	2.4	1.9	2.3		2.0	1.8	2.2	2.2
	Instant of max (ms)	4.5		4.4		4.6		4.5	
		1st impact	2nd impact	1st impact	2nd impact	1st impact	2nd impact	1st impact	2nd impact
Pressure under the roof	Max. pressure (MPa)	18.0	7.2			3.0	8.0	centre: 4.0 else: 7.0	centre: 25. else: 5.0
	Instant of max (ms)	2.1	4 to 5			2.2	4 to 5	2.1	3.5 to 6

As for pressure under the roof, the CASTEM-PLEXUS and EUROPLEXUS simulations are able to represent the two experimental peaks. The instant of the maximal pressure for each peak coincides perfectly with the experimental results, but the amplitude of the peak is not correct. The computed first peak is much lower and much larger than the experimental one (from 4 MPa in the centre to 7 MPa at the roof edge in the EUROPLEXUS simulation, instead of 18 MPa in the test).

On the contrary, for the second peak, the computation shows a high and thin peak in the centre (maximal pressure: 25 MPa) and larger peaks elsewhere (maximal pressure: 5 MPa) whereas the test presents a succession of small peaks. At one quarter of the radius and at mid-radius, the top value of the newly simulated second peak presents a good similarity with the experimental values.

On the symmetry axis, the second peak has a very different shape from anywhere else under the roof. The amplitude of the computed second peak in the centre of the roof is a consequence of the high vertical speeds observed for the fluid on the symmetry axis.

As EUROPLEXUS computes the roof displacement correctly, the global impulse on the roof must be correct. On the one hand, Cariou [6] indicates that the pressure measurement in the mock-up lacks precision, which could partially explain the differences between the computed and the experimental results. On the other hand, as pressure computed with SIRIUS is not available in [12], it is difficult to assess the precision of the simulation without reliable reference data.

Globally, the EUROPLEXUS simulation is in better agreement with the experimental results than the CASTEM-PLEXUS one. The comparison with the SIRIUS results show that, in some cases, the EUROPLEXUS results are better than the SIRIUS ones and, in other cases, the SIRIUS results are closer to the experimental ones. Generally speaking, the three sets of numerical results are in good agreement with the test.

7. Discussion

In this part, a synthesis of the results computed with the current EUROPLEXUS model is presented.

Initially, air and water are at atmospheric pressure whereas the central bubble contains gas at high pressure. All fluids are at rest. The gas contained in the bubble begins expanding immediately, and a pressure wave propagates spherically.

Water and the bubble gas are expelled from the central part of the mock-up. The pressure wave impacts the vessel base at 0.14 ms, which causes a local downward lowering of the vessel.

From 0.14 ms to 0.22 ms, the pressure wave moves laterally and impacts the lower part of the lateral wall from the bottom right-hand corner to mid-height. The lateral wall begins moving sideways from 0.2 ms, thus initiating the formation of a lower bulge. Even if the vessel base undergoes a stress increase, strains remain elastic.

Between 0.22 ms and 0.5 ms, the pressure wave is pushed back by the lateral wall towards the upper part of the mock-up with a fluid speed oriented diagonally. The gaseous central zone now fills one third of the mock-up.

Near the symmetry axis, the air layer is compressed against the roof by the liquid thrown upwards. Pressure increases slightly under the roof. Simultaneously there is the creation of the lower bulge in the lateral wall and the downward bending of the vessel base. The whole vessel is submitted to a stress increase, but particularly in the bottom right-hand corner.

From 0.5 to 1.5 ms, the gaseous central zone goes on expanding in a spherical shape. The water in the lower part of the mock-up continues to move downwards and to impact the vessel base. Disorganised water motion occurs near the bottom right-hand corner. Progressively, the fluid near the lateral wall flows upwards. The fluid flows induce a stress increase in the vessel base and in the lateral wall and the appearance of plastic strains in the vessel base, in the bottom right-hand corner and in the lateral wall. The lower bulge formation and the lowering of the base continue.

Meanwhile, there is a massive arrival of water towards the roof and some steam trails appear not far from the lateral wall, after the pressure wave rebound causes local depressurisation. The air layer is compressed below the roof and pushed horizontally towards the top right-hand corner.

Between 1.5 and 3.5 ms, the water along the lateral wall flows vertically upwards. A globally upward rotating fluid flow forms around the bubble. Water impacts the roof vertically. Air is concentrated in the top right-hand corner and the air zone reaches a minimal size after 3 ms.

The vessel base and the lower bulge continue to deform. Plastic strains increase in the vessel base and remain constant at the level of the lower bulge. Due to the water thrust, the roof suffers a first pressure peak and an upward deformation starting in the centre and progressing laterally. Stresses increase in the centre of the roof. Owing to the compression of the air in the top right-hand corner and the massive arrival of water directed upward along the lateral wall, the lateral wall starts bending just below the top right-hand corner.

Between 4 and 5 ms, the central gaseous zone reaches the bottom of the mock-up, but a liquid layer still exists along the vessel base. In the top corner, water impacts the vessel perpendicularly, which causes the formation of the upper bulge in the lateral wall and of a plastic hinge at the junction between the roof and the vessel. Stresses increase at the level of the upper bulge, and plastic strains appear.

There is a general upward water and bubble gas flow in the whole mock-up, except in the top right-hand corner. The main consequences of this massive water flow are the formation of a second pressure peak under the roof and a general deformation of the roof. At the same time, the air bag in the top right-hand corner is thrust along the walls: horizontally along the roof and downwards along the vessel.

Later, there is a progressive decrease of the water speed and a flowing back of the air in the corner. Consequently the air zone is extended. Because of the pressure decrease in the lower part of the vessel, the vessel base goes slightly back upwards.

8. Conclusion

In this paper, a computation of the MARA 8 test simulating a Hypothetical Core Disruptive Accident is presented. The test consists in an explosion inside a steel vessel covered with a flexible roof. An explosive charge is placed in the middle of the mock-up. The vessel is filled with water, topped by an air layer below the roof. A specific HCDA constitutive law has been developed in the EUROPLEXUS code to simulate this kind of explosion.

The code computes successfully the explosion during 7 ms of physical time. The simulation shows the propagation of a pressure wave from the explosive zone towards the external vessel. A large gaseous zone is created in the middle of the mock-up. The pressure wave impacts first the vessel base and then the lateral wall. A large lower bulge forms in the lower part of the lateral wall of the vessel.

Water is pushed then back by the vessel, flows upward and impacts the roof. The roof undergoes a high pressure peak and is raised. The air layer is expelled in the top right-hand corner by the upward flow of the water. A second bulge appears in the upper part of the lateral wall.

A comparison has been undertaken between the experimental results, the results of the EUROPLEXUS simulation and previous ones computed by the CASTEM-PLEXUS code and by the SIRIUS code. Globally the results of the three simulations are in good agreement with the test results. Apart from the pressure computed under the roof, the new results of the EUROPLEXUS code more closely match the experimental results than do the previous ones.

References

[1] D. Acker, A. Benuzzi, A. Yerkess, J. Louvet. MARA 01/02 – Experimental validation of the SEURBNUK and SIRIUS containment codes. In: J. Rastoin, ed., *6th Int. Conf. on Structural Mechanics In Reactor Technology*, paper E3/6. Int. Association for Structural Mechanics in Reactor Technology and Commission of the European Communities, Luxembourg, 1981.

[2] C. Albertini et al. The JRC-COVA programme: Final Report. Commission of the European Communities, Report EUR 8705. *Nuclear Science and Technology*: 1–182, 1984.

[3] A. Benuzzi. Comparison of different LMFBR primary containment codes applied to a benchmark problem. *Nuclear Engineering and Design*, **100**: 239–249, 1987.

[4] Y. Blanchet, P. Obry, J. Louvet. Treatment of fluid–structure interaction with the SIRIUS computer code. In: J. Rastoin, ed., *Proc. 6th Int. Conf. on Structural Mechanics In Reactor Technology*, paper B8/8. Int. Association for Structural Mechanics in Reactor Technology and Commission of the European Communities, Luxembourg, 1981.

[5] C. Bour, M. Spérandio, J. Louvet, C. Rieg. LMFBR's core disruptive accident. Mechanical study of the reactor block. In: A.H. Hadjian, ed., *Proc. 10th Int. Conf. on Structural Mechanics In Reactor Technology*, Vol. E, 281–287. American Association for Structural Mechanics in Reactor Technology, Los Angeles, USA, 1989.

[6] Y. Cariou, M. Spérandio, M. Lepareux, K. Christodoulou. LMFBR's whole core accident. Validation of the PLEXUS code by comparison with MARA tests. In: K.F. Kussmaul, ed., *Proc. 12th Int. Conf. on Structural Mechanics In Reactor Technology*, Vol. E, 209–214. Int. Association for Structural Mechanics in Reactor Technology, Amsterdam, Netherlands, 1993.

[7] Y. Cariou, J.P. Pirus, C. Avallet. LMR large accident analysis method. In: M. Livolant, ed., *Proc. 14th Int. Conf. on Structural Mechanics In Reactor Technology*, Vol. P, 395–402. Int. Association for Structural Mechanics in Reactor Technology and Commissariat à l'Energie Atomique, Paris, France, 1997.

[8] F. Casadei, A. Daneri, G. Toselli. Use of PLEXUS as a LMFBR primary containment code for the CONT benchmark problem. In: A.H. Hadjian, ed., *Proc. 10th Int. Conf. on Structural Mechanics In Reactor Technology*, Vol. E, 299–304. American Association for Structural Mechanics in Reactor Technology, Los Angeles, USA, 1989.

[9] C. Chavant, A. Hoffmann, P. Verpeaux, J. Dubois. Plexus: A general computer code for explicit Lagrangian computation. In: T.A. Jaeger, ed., *Proc. 5th Int. Conf. on Structural Integrity In Reactor Technology*, paper B2/8. Int. Association for Structural Mechanics in Reactor Technology and Commission of the European Communities, Luxembourg, 1979.

[10] A. Daneri et al. Influence of the representation models of the stress–strain law on the LMFBR structures in an HCDA. In: J. Rastoin, ed., *Proc. 6th Int. Conf. on Structural Integrity In Reactor Technology*, paper E4/4. Int. Association for Structural Mechanics in Reactor Technology and Commission of the European Communities, Luxembourg, 1981.

[11] F. David. Etude d'une composition explosive flegmatisée. Applications à la déformation d'une cuve. In: *Proc. Symposium sur les hautes pressions dynamiques*. Paris, France, 1978.

[12] C. Fiche, J. Louvet, B.L. Smith, A. Zucchini. Theoretical experimental study of flexible roof effects in an HCDA's simulation. In: J. Stalpaert, ed., *Proc. 8th Int. Conf. on Structural Integrity In Reactor Technology*, Vol. E, 139–144. Commission of the European Communities and Int. Association for Structural Mechanics in Reactor Technology, Luxembourg, 1985.

[13] A. Hoffmann, M. Lepareux, B. Schwab, H. Bung. Plexus – A general computer program for fast dynamic analysis. In: *Proc. Conf. on Structural Analysis and Design on Nuclear Power Plant*. Porto Alegre, Brazil, 1984.

[14] H. Holtbecker. Testing philosophy and simulation techniques. *Nuclear Engineering and Design*, **42**: 75–87, 1977.

[15] N.E. Hoskin, M.J. Lancefield. The COVA programme for the validation of computer codes for fast reactor containment studies. *Nuclear Engineering and Design*, **46**: 17–46. 1978.

[16] K.C. Kendall, A. Benuzzi. The COVA programme: Validation of the fast reactor containment code SEURBNUK. *Nuclear Engineering and Design*, **57**: 79–105, 1980.

[17] K.C. Kendall, D.J. Adnams. Experiments to validate structural dynamics code used in fast reactor safety assessment. *Science and Technology of Fast Reactor Safety*, Vol. 2. British Nuclear Energy Society, London, England, 1986.

[18] M. Lepareux, B. Schwab, A. Hoffmann, P. Jamet, H. Bung. Un programme général pour l'analyse dynamique rapide – Cas des tuyauteries. In: *Proc. Colloque Tendances Actuelles en Calcul des Structures*. Bastia, France, 1985.

[19] M. Lepareux, B. Schwab, H. Bung. Plexus: A general computer program for the fast dynamic analysis – The case of pipe circuits. In: J. Stalpaert, ed., *Proc. 8th Int. Conf. on Structural Mechanics In Reactor Integrity*, Vol. F1, 39–46. Commission of the European Communities and Int. Association for Structural Mechanics in Reactor Technology, Luxembourg, 1985.

[20] M. Lepareux, H. Bung, A. Combescure, J. Aguilar. Analysis of a CDA in a LMFBR with a multiphasic and multicomponent behaviour law. In: H. Shibata, ed., *Proc. 11th Int. Conf. on Structural Mechanics In Reactor Integrity*, Vol. E, 371–376. Atomic Energy Society of Japan and Int. Association for Structural Mechanics in Reactor Technology, Tokyo, Japan, 1991.

[21] M. Lepareux, H. Bung, A. Combescure, J. Aguilar, J.F. Flobert. Analysis of an HCDA in a fast reactor with a multiphase and multicomponent behavior law. In: K. Kussmaul, ed., *Proc. 12th Int. Conf. on Structural Mechanics In Reactor Integrity*, Vol. E, 197–202. Int. Association for Structural Mechanics in Reactor Technology, Amsterdam, Netherlands, 1993.

[22] M. Lepareux, J.M. Michelin, D. Thiault. Plexus-R : une extension de Plexus à la robotique. CEA report DMT/94-138, 1994.

[23] J. Louvet, P. Hamon, B.L. Smith, A. Zucchini. MARA 10: an integral model experiment in support of LMFBR containment analysis. In: F.H. Wittmann, ed., *Proc. 9th Int. Conf. on Structural Mechanics In Reactor Integrity*, Vol. E, 331–337. A.A. Balkema, Rotterdam, Netherlands, 1987.

[24] J. Louvet. Containment response to a core energy release. Main experimental and theorical issues – Future trends. In: A.H. Hadjian, *Proc. 10th Int. Conf. on Structural Mechanics In Reactor Integrity*, Vol. E, 305–310. American Association for Structural Mechanics in Reactor Technology, Los Angeles, USA, 1989.

[25] M.F. Robbe, M. Lepareux, H. Bung. *Plexus – Notice théorique.* CEA report DMT/94-490, 1994.

[26] M.F. Robbe, M. Lepareux, N. Vivien, G. Cénérino. Screening calculations on the vessel lower head behaviour due to an in-vessel steam explosion. In: M. Livolant, ed., *Proc. 14th Int. Conf. on Structural Mechanics In Reactor Technology*, Vol. P, 451–458. Int. Association for Structural Mechanics in Reactor Technology and Commissariat à l'Energie Atomique, Paris, France, 1997.

[27] M.F. Robbe, P. Galon, T. Yuritzinn. Castem-Plexus: Un logiciel de dynamique rapide pour évaluer l'intégrité des structures en cas d'accident. In: J. Fabri, ed., *Proc. 4th Conf. INSTRUC.* Société Française des Mécaniciens, Courbevoie, France, 1999.

[28] M.F. Robbe, M. Lepareux. Scoping calculations of an in-vessel steam explosion. CASTEM-PLEXUS computations. In: *Proc. 8th Int. Conf. On Nuclear Engineering*, paper 8269, CD-rom. American Society of Mechanical Engineers, New York, USA, 2000.

[29] M.F. Robbe, M. Lepareux. Estimation of the mechanical consequences of an in-vessel steam explosion by means of parametric computations. In: V. Kompiš, ed., *Proc. 8th International Conference on Numerical Methods in Continuum Mechanics*, CD-rom. University of Žilina, Žilina, Slovak Republic, 2000.

[30] M.F. Robbe, M. Lepareux, C. Trollat. Assessment of the hydrodynamic loads due to a LOCA in a 3-loop PWR. Pipe computations with the code CASTEM-PLEXUS. In: V. Kompiš, ed., *Proc. 8th Int. Conf. On Numerical Methods in Continuum Mechanics*, CD-rom. University of Žilina, Žilina, Slovak Republic, 2000.

[31] M.F. Robbe, Y. Cariou, M. Lepareux, E. Treille. Numerical simulation of a Hypothetical Core Disruptive Accident in the MARA 8 mock-up with the CASTEM-PLEXUS computer code. In: V. Kompiš, ed., *Proc. Int. Conf. on Numerical Methods in Continuum Mechanics 2000*, CD-rom. University of Žilina, Žilina, Slovak Republic, 2000.

[32] M.F. Robbe, Y. Cariou, M. Lepareux, E. Treille. Validation of the Core Disruptive Accident constitutive law of the Castem-Plexus code on the Mara8 test. In: H. Nguyen-Dang, ed., *Proc. Int. Colloquium in Mechanics of Solids, Fluids, Structures and Interactions.* LTAS – Université de Liège, Liège, Belgique, 2000.

[33] M.F. Robbe, N. Vivien, M. Valette, E. Berglas. Use of thermalhydraulic and mechanical linked computations to estimate the mechanical consequences of a steam explosion. *Journal of Mechanical Engineering*, **52**: 65–90, 2001.

[34] M.F. Robbe, M. Lepareux, E. Treille, Y. Cariou. Numerical simulation of a Core Disruptive Accident and comparison with the simple test Mara 8. In: D. Todd, ed., *Proc. ANS/HPS Student Conference "2001: A nuclear odyssey"*, CD-rom. American Nuclear Society, USA, 2001.

[35] M.F. Robbe, M. Lepareux. Evaluation of the mechanical consequences of a steam explosion in a nuclear reactor. *Bulgarian Journal of Theoretical and Applied Mechanics*, in print, 2002.

[36] M.F. Robbe, M. Lepareux, C. Trollat. Hydrodynamic loads on a PWR primary circuit due to a LOCA. *Nuclear Engineering and Design*, **211**(2-3): 189–228, 2002.

[37] J.E.A. Sidoli, K.C. Kendall. The WINCON programme – Validation of the fast reactor primary containment codes. In: D.G. Walton, ed., *Proc. INE Int. Conf. On Nuclear Containment.* Nuclear Containment Structures, Cambridge University Press, 1988.

[38] B.L. Smith, C. Fiche, J. Louvet, A. Zucchini. A code comparison exercise based on the LMFBR containment experiment MARA-04. In: J. Stalpaert, ed., *Proc. 8th Int. Conf. on Structural Mechanics In Reactor Technology*, Vol. E, 151–157. Commission of the European Communities and Int. Association for Structural Mechanics in Reactor Technology, Luxembourg, 1985.

[39] E. Struder, P. Galon. Hydrogen combustion loads Plexus calculations. *Nuclear Engineering and Design*, **174**: 119–134, 1997.

[40] H.U. Wenger, B.L. Smith. On the origin of the discrepancies between theory and experiment in the COVA series. In: F.H. Wittmann, ed., *Proc. 9th Int. Conf. on Structural Mechanics In Reactor Technology*, Vol. E, 339–344. A.A. Balkema, Rotterdam, Netherlands, 1987.